

# Topological phase transitions with and without energy gap closing

Yunyou Yang<sup>1</sup>, Huichao Li<sup>1</sup>, L. Sheng<sup>1,\*</sup>, R. Shen<sup>1</sup>, D. N. Sheng<sup>2</sup>, and D. Y. Xing<sup>1†</sup>

<sup>1</sup>*National Laboratory of Solid State Microstructures and Department of Physics, Nanjing University, Nanjing 210093, China*

<sup>2</sup>*Department of Physics and Astronomy, California State University, Northridge, California 91330, USA*

(Dated: January 9, 2013)

Topological phase transitions in a three-dimensional (3D) topological insulator (TI) with an exchange field of strength  $g$  are studied by calculating spin Chern numbers  $C^\pm(k_z)$  with momentum  $k_z$  as a parameter. When  $|g|$  exceeds a critical value  $g_c$ , a transition of the 3D TI into a Weyl semimetal occurs, where two Weyl points appear as critical points separating  $k_z$  regions with different first Chern numbers. For  $|g| < g_c$ ,  $C^\pm(k_z)$  undergo a transition from  $\pm 1$  to 0 with increasing  $|k_z|$  to a critical value  $k_z^C$ . Correspondingly, surface states exist for  $|k_z| < k_z^C$ , and vanish for  $|k_z| \geq k_z^C$ . The transition at  $|k_z| = k_z^C$  is accompanied by closing of spin spectrum gap rather than energy gap.

PACS numbers: 72.25.-b, 73.23.-f, 73.50.-h, 73.20.At

The quantum Hall (QH) effect [1, 2] in a two-dimensional (2D) electron gas under a strong magnetic field provided the first example of topological state of matter in condensed matter physics, which cannot be described by the Landau theory of symmetry breaking. Thouless, Kohmoto, Nightingale, and Nijs (TKNN) revealed that the essential character of a QH insulator, different from an ordinary insulator, is a topological invariant of occupied electron states [3] or many-body wavefunctions [4]. They related the Hall conductivity of the system to the first Chern number (or TKNN number), which is quantized when the Fermi level lies in an energy gap between Landau levels. In such systems, topological phase transitions can happen only by closing the energy gap. Gapless edge states must appear on the boundary between a QH insulator and an ordinary insulator, which is ensured by the topological invariant. Interestingly, Haldane [5] proposed a spinless electron model on a 2D honeycomb lattice with staggered magnetic fluxes to realize the topological QH effect without Landau levels.

The quantum spin Hall (QSH) effect was first theoretically predicted by Kane and Mele [6] and by Bernevig and Zhang [7], and then experimentally observed in HgTe quantum wells. [8, 9] Unlike the QH systems, where time-reversal (TR) symmetry must be broken, the QSH systems preserve the TR symmetry. The main ingredient is the existence of strong spin-orbit coupling, which acts as spin-dependent magnetic fluxes coupled to the electron momentum. The QSH state is characterized by a bulk band gap and gapless helical edge states on the sample boundary. [6–11] The existence of the edge states is due to nontrivial topological properties of bulk energy bands. However, the bulk band topology of the QSH systems cannot be classified by the first Chern number, which always vanishes. Instead, it is classified by new topological invariants, namely, the  $Z_2$  index [12] or the spin Chern numbers. [13–15] For TR-invariant systems, both  $Z_2$  and spin Chern numbers were found to give an equivalent description. [14, 15] The robustness of the  $Z_2$  index relies on the presence of the TR symmetry. In contrast, the

spin Chern numbers remain to be integer-quantized, independent of any symmetry, as long as both the band gap and spin spectrum gap stay open. [14] They are also different from the first Chern number for the QH state, which is protected by the bulk energy gap alone. The spin Chern numbers have been employed to study the TR-symmetry-broken QSH effect. [16]

The QSH system is an example of the 2D topological insulators (TIs). Its generalization to higher dimension led to the birth of 3D TIs. [17–21] A 3D TI has a bulk band gap and surface states on the sample boundary. The metallic surface states provide a unique platform for realizing some exotic physical phenomena, such as Majorana fermions [22] and topological magnetoelectric effect. [23, 24] The 3D TIs have been experimentally observed in  $\text{Bi}_{1-x}\text{Sb}_x$ ,  $\text{Bi}_2\text{Te}_3$ , and  $\text{Bi}_2\text{Se}_3$  materials, [25–30] which greatly stimulates the research in this field. The 3D TIs with TR symmetry are usually classified by four  $Z_2$  indices, [17, 18] and are divided into two general classes: strong and weak TIs, depending on the sum of the four  $Z_2$  indices. In the presence of disorder, while the weak TIs are unstable, the strong TIs remain to be robust. The  $Z_2$  indices are essentially defined only on the TR-symmetric planes in the Brillouin zone, and do not provide information about the distribution of surface states in the full momentum space. When the TR symmetry is broken, the  $Z_2$  indices become invalid. Therefore, a more general characterization scheme for the bulk band topology, which does not rely on any symmetry and can provide more information about the distribution of surface states, is highly desirable.

In this Letter, for a 3D TI with an exchange field of strength  $g$ , we consider a momentum component, e.g.,  $k_z$ , as a parameter, and analytically calculate spin Chern numbers  $C^\pm(k_z)$  for the effective 2D system. The phase diagram for  $C^\pm(k_z)$  obtained can describe the systematic evolution of the bulk band topology of the 3D TI with varying parameters, and provide more information about the surface states. For small  $g$ ,  $C^\pm(k_z)$  take values  $\pm 1$  for  $|k_z| < k_z^C$ , and undergo a transition to 0 at  $|k_z| = k_z^C$ .

Correspondingly, on a sample surface parallel to the  $z$ -axis, helical surface states exist in the region  $|k_z| < k_z^C$ , and disappear for  $|k_z| \geq k_z^C$ . At  $|k_z| = k_z^C$ , the spin spectrum gap closes, but the energy gap remains open, which is distinct from a usual topological phase transition, where the energy gap always collapses. When  $|g|$  is greater than a critical value  $g_c$ , a topological transition of the 3D TI into a Weyl semimetal occurs. Two Weyl points appear as critical points separating a QH phase of the effective 2D system for  $|k_z| < k_z^W$  from an ordinary insulator phase for  $|k_z| > k_z^W$ , indicating that their appearance is topological rather than accidental. Chiral surface states existing in the region  $|k_z| < k_z^W$  give rise to the Fermi arcs.

Let us start from the effective Hamiltonian proposed in Ref. [19]:  $H = A_2\tau_x(k_x\sigma_x + k_y\sigma_y) + M(\mathbf{k})\tau_z + A_1k_z\tau_x\sigma_z + g\sigma_z$ , which was used to describe the strong TI of  $\text{Bi}_2\text{Se}_3$ . Here,  $\sigma_m$  and  $\tau_m$  ( $m = x, y$  or  $z$ ) denote the Pauli matrices in spin and orbital spaces, and  $M(\mathbf{k}) = M_0 - B_1k_z^2 - B_2k_\perp^2$  with  $k_\perp^2 = k_x^2 + k_y^2$  is the mass term expanded to the second order. In the last term, we include an exchange field of strength  $g$ , in order to study the TR-symmetry-broken effect on topological properties of the TI. For convenience, the momentum is set to be dimensionless, by properly choosing the units of parameters in the model, namely,  $M_0$ ,  $A_1$ ,  $A_2$ ,  $B_1$ , and  $B_2$ .

Making a unitary transformation  $\mathcal{H} = U^\dagger H U$  with  $U = \frac{1}{2}(1 + \tau_x) + \frac{1}{2}(1 - \tau_x)\sigma_z$ , we obtain

$$\mathcal{H} = A_2(k_x\sigma_x + k_y\sigma_y) + [M(\mathbf{k})\tau_z + A_1k_z\tau_x + g]\sigma_z. \quad (1)$$

The eigenstates of Hamiltonian (1) can be easily solved by first diagonalizing the operator in the square bracket. The four eigenenergies are obtained as

$$E_{\pm}^{v(c)}(\mathbf{k}) = -(+)\sqrt{A_2^2k_\perp^2 + [g \pm \lambda(\mathbf{k})]^2}, \quad (2)$$

where  $\lambda(\mathbf{k}) = \sqrt{M^2(\mathbf{k}) + A_1^2k_z^2}$ , and subscripts  $\pm$  indicate two valence (conduction) bands with superscript  $v$  ( $c$ ). The electron wavefunctions in the valence bands are given by

$$\varphi_{\pm}(\mathbf{k}) = \phi_{\pm}(\mathbf{k}) \otimes \chi_{\pm}(\mathbf{k}). \quad (3)$$

Here,  $\phi_+(\mathbf{k}) = [\text{sgn}(A_1k_z) \cos \alpha_k, \sin \alpha_k]^T$  and  $\phi_-(\mathbf{k}) = [\text{sgn}(A_1k_z) \sin \alpha_k, -\cos \alpha_k]^T$  are wavefunctions in the  $\tau_z$  space, and  $\chi_{\pm} = (\frac{k_x - ik_y}{k_\perp} \sin \theta_k^\pm, -\cos \theta_k^\pm)^T$  are wavefunctions in the  $\sigma_z$  space, with  $2\alpha_k = \text{ctg}^{-1}[M(\mathbf{k})/|A_1k_z|]$  and  $2\theta_k^\pm = \text{ctg}^{-1}[(g \pm \lambda(\mathbf{k}))/(A_2k_\perp)]$ .

The basic idea of our theoretical calculation is explained as follows. We consider one of the momentum components, e.g.,  $k_z$  as a parameter. For a given  $k_z$ , Eq. (1) is equivalent to a 2D system, for which spin Chern numbers  $C^\pm(k_z)$  can be defined. For a semi-infinite sample of the 3D TI with its surface parallel to the  $z$  axis,  $k_z$

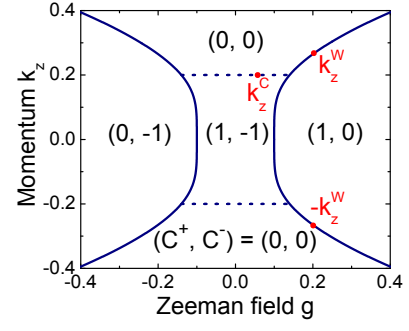


FIG. 1: Phase diagram determined from spin Chern numbers in the  $k_z$ - $g$  plane. The parameters are chosen to be  $M_0 = 0.1$ ,  $A_1 = 0.7$ ,  $A_2 = 1$ ,  $B_1 = 2.5$ , and  $B_2 = 14$ .

remains to be a good quantum number. Correspondingly, nonzero  $C^\pm(k_z)$  indicate that edge states with the given  $k_z$  must appear on the edge of the effective 2D system. The edge states at various  $k_z$  essentially form surface states of the 3D sample. Therefore, the characteristics of the surface states can be determined from the calculation of the  $k_z$ -dependent spin Chern numbers  $C^\pm(k_z)$ .

The spin Chern numbers for the effective 2D system are calculated in a standard way, which has been described in details in previous works. [15, 16] By studying a special case of  $k_z = 0$ , we find that the topological properties of Eq. (1) can be described by the spin Chern numbers  $C^\pm(k_z)$  associated with  $\tau_z$ . Here,  $\tau_z$  corresponds to  $U\tau_zU^\dagger = \tau_z\sigma_z$  in the original Hamiltonian  $H$ , and so can be considered as a spin operator, measuring the difference of spin polarization between the two orbits. The eigenstates of projected spin operator  $P\tau_zP$  need to be calculated first, where  $P$  is the projection operator into the valence bands. Since  $P\tau_zP$  commutes with momentum operator, its eigenstates can be obtained at each momentum  $\mathbf{k}$  separately. The eigenvalues of  $P\tau_zP$  are given by

$$\xi^\pm(\mathbf{k}) = \pm\sqrt{\cos^2 2\alpha_k + \cos^2(\theta_k^+ - \theta_k^-) \sin^2 2\alpha_k}. \quad (4)$$

The corresponding eigenfunctions are denoted by  $\Psi^\pm(\mathbf{k})$ , whose expressions are lengthy and will not be written out here. The spin Chern numbers are just the Chern numbers of the two spin sectors formed by  $\Psi^\pm(\mathbf{k})$ , i.e.,  $C^\pm(k_z) = \frac{i}{2\pi} \int dk_x dk_y \hat{\mathbf{e}}_z \cdot [\nabla_2 \times \langle \Psi^\pm(\mathbf{k}) | \nabla_2 | \Psi^\pm(\mathbf{k}) \rangle]$ , where  $\nabla_2$  is the 2D Laplace operator acting on  $(k_x, k_y)$ . By some algebra,  $C^\pm(k_z)$  are derived to be

$$C^\pm(k_z) = \pm \frac{1}{2} \left[ \text{sgn}(B_2) + \text{sgn}(Q(k_z) \text{sgn}[P(k_z)] \pm g) \right] \quad (5)$$

with  $P(k_z) = M_0 - B_1k_z^2$  and  $Q(k_z) = \sqrt{P^2(k_z) + A_1^2k_z^2}$ .

Equations (2), (4), and (5) are the main analytical results of this work. For  $g = 0$ , the spin Chern numbers at  $k_z = 0$  reduces to  $C^\pm(0) = \pm \frac{1}{2} [\text{sgn}(B_2) + \text{sgn}(M_0)]$ .  $C^\pm(0)$  are nonzero when  $B_2$  and  $M_0$  have the same sign,

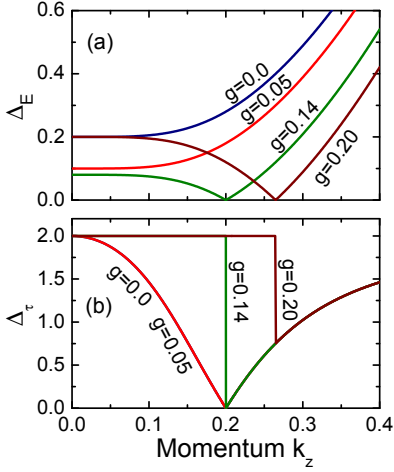


FIG. 2: Energy gap  $\Delta_E$  (a) and spin spectrum gap  $\Delta_\tau$  (b) as functions of momentum  $k_z$  for different values of  $g$ . The other parameters are the same as in Fig. 1.

and vanish otherwise.  $C^\pm(0)$  play a role similar to the  $Z_2$  index. Nonzero  $C^\pm(0)$  ensure that surface states exist in the vicinity of  $k_z = 0$  on a surface parallel to the  $z$  axis. Without loss of generality, we will focus on the parameter region of  $B_2 > 0$  and  $M_0 > 0$ , to which  $\text{Bi}_2\text{Se}_3$  belongs. We wish to emphasize here that when  $k_z$  is considered as a parameter, the effective 2D Hamiltonian (1) breaks the TR symmetry for any  $k_z \neq 0$ , even if  $g = 0$ , as its TR counterpart is at  $-k_z$ . Therefore, while the  $k_z$ -dependent spin Chern numbers given by Eq. (5) remain to be valid at any  $k_z$ , a  $Z_2$  index cannot be defined for any  $k_z \neq 0$ . Eq. (5) allows us to extract more information about the basic characteristics of the surface states.

A typical phase diagram for the spin Chern numbers in the  $k_z$  versus  $g$  plane, as determined by Eq. (5), is plotted in Fig. 1. For simplicity,  $A_2$  is taken to be the unit of energy. For small  $|g|$ ,  $C^\pm(k_z) = \pm 1$  at small  $|k_z|$ , corresponding to a QSH phase of the effective 2D system, and drop to 0 with increasing  $|k_z|$  to a critical value  $k_z^C = \sqrt{M_0/B_1}$ , as indicated by the dotted lines. The system becomes an ordinary insulator for  $|k_z| > k_z^C$ . When  $|g|$  is greater than a critical value  $g_c$ , the effective 2D system enters a QH phase with a nonzero total (first) Chern number  $C(k_z) \equiv C^+(k_z) + C^-(k_z) = 1$  if  $g > 0$ , and  $-1$  if  $g < 0$ . The boundary enclosing this phase is determined by equation  $g = \pm Q(k_z)$ , as indicated by the solid curves. The critical exchange field is given by  $g_c = \min[Q(k_z)]$ , and  $g_c \simeq 0.1$  for the parameters used in Fig. 1.

It is interesting to see how the energy gap  $\Delta_E(k_z) = \min[E_\pm^c(\mathbf{k}) - E_\pm^v(\mathbf{k})]|_{k_z}$  and the spin spectrum gap  $\Delta_\tau(k_z) = \min[\xi^+(\mathbf{k}) - \xi^-(\mathbf{k})]|_{k_z}$  behave on the boundary (solid and dashed lines) between different phases. From Eqs. (2) and (4), we find that on the dotted lines in Fig. 1, the spin spectrum gap closes at  $k_x = k_y = 0$ , but the energy gap remains open. On the contrary, on the solid

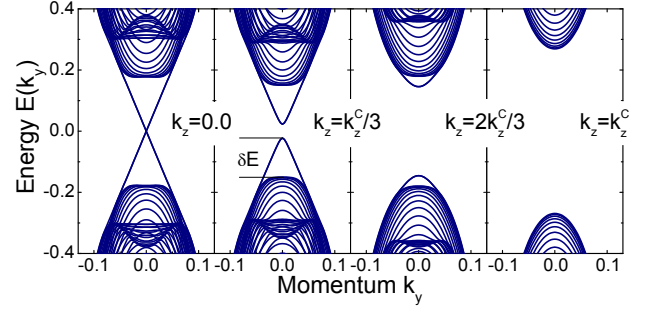


FIG. 3: Profiles of energy spectrum for a semi-finite sample of the 3D TI for four different  $k_z$  at  $g = 0.05$ . The other parameters are the same as in Fig. 1.

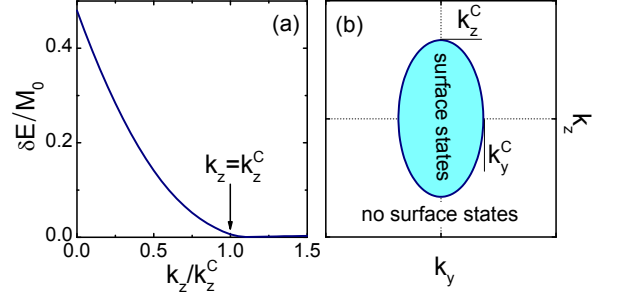


FIG. 4: (a) Maximum level spacing  $\delta E$  between the edge states and bulk states as a function of  $k_z/k_z^C$ . (b) A schematic of the distribution of surface states in 2D momentum space.

boundary lines, the energy gap closes at  $k_x = k_y = 0$ , but the spin spectrum gap remains open.  $\Delta_E$  and  $\Delta_\tau$  as functions of  $k_z$  for several values of  $g$  are plotted in Figs. 2(a) and 2(b), respectively. We notice that at  $g = 0.14$  and  $k_z = k_z^C = 0.2$ , the energy gap and spin spectrum gap vanish simultaneously. This is because the dotted and solid boundary lines in Fig. 1 intersect just at that point.

To study the surface states directly, we construct a tight binding model on a cubic lattice with two spins and two orbits on each site, which recovers the Hamiltonian Eq. (1) in the continuum limit. A semi-infinite sample with its surface parallel to the  $y$ - $z$  plane is considered, where  $k_y$  and  $k_z$  remain to be good quantum numbers. The calculated energy spectrum for  $g = 0.05$  is plotted as a function of  $k_y$  for four different values of  $k_z$  in Fig. 3. Although  $g \neq 0$  breaks the TR symmetry, the surface states remain to be gapless at  $k_z = 0$ , because  $\tau_z$  in Eq. (1) is conserved at  $k_z = 0$ . From Fig. 3, it is found that for  $k_z = 0, k_z^C/3$ , and  $2k_z^C/3$ , surface states always exist in the bulk energy gap, but no surface states appear at  $k_z = k_z^C$ . To see the evolution of surface states with  $k_z$  more clearly, we define a maximum level spacing  $\delta E$  between the surface states and bulk states, as illustrated in Fig. 3. In Fig. 4(a),  $\delta E$  is plotted as a function of  $k_z$ . One can see that  $\delta E$  decreases with increasing  $k_z$ , and drops to nearly 0 at  $k_z \geq k_z^C$ . Therefore, we conclude

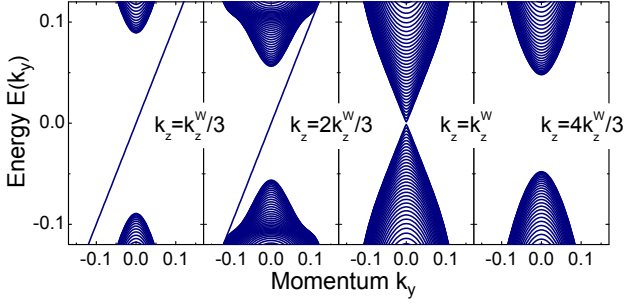


FIG. 5: Profiles of energy spectrum of a semi-finite sample for four different  $k_z$  at  $g = 0.2$ . The other parameters are the same as in Fig. 1.

that surface states exist only in the region  $|k_z| < k_z^c$ , and vanish for  $|k_z| \geq k_z^c$ , which is well consistent with the phase diagram of Fig. 1.

The critical momentum  $k_z^c$  marks a topological phase transition, characterized by the change in the spin Chern numbers, with disappearance of surface states as an observable consequence. This topological phase transition is unconventional, which is accompanied by closing the spin spectrum gap rather than the energy gap. While the closing of the spin spectrum gap may not be observed directly, we find that the average of operator  $\tau_z$  in  $H$ , namely,  $\sum_{\beta=\pm} \langle \varphi_{\beta}(\mathbf{k}) | U^\dagger \tau_z U | \varphi_{\beta}(\mathbf{k}) \rangle \propto \cos(2\alpha_k)$ , changes its sign at  $\mathbf{k} = (0, 0, \pm k_z^c)$ , which indicates a reversal of the orbital polarization, leading to a bulk physical observable at the transition. For the strong TI under consideration, the nontrivial bulk band topology can be examined in any direction. For example, by considering  $k_y$  as a parameter, we can calculate the spin Chern numbers in the effective 2D space of  $(k_x, k_z)$ , and obtain a critical  $k_y^c = \sqrt{M_0/B_2}$ . Combining  $k_y^c$  and  $k_z^c$  together, we can depict the region in the  $k_y$ - $k_z$  plane, where topological surface states exist on a surface parallel to the  $y$ - $z$  plane, as shown in Fig. 4(b).

For  $|g| > g_c$ , the 3D system enters another topological phase characterized by a nonzero total Chern number  $C(k_z)$  for small  $|k_z|$ , which is essentially a Weyl semimetal phase. [31–34] The quantum phase transition from the 3D TI to the Weyl semimetal with tuning  $g$  can be understood as a topological transition, at which the energy gap closing causes one of spin Chern numbers  $C^\pm(k_z)$  to vanish, while the other remains to be quantized. At a given  $g$ , from equation  $g = \pm Q(k_z)$  for the solid boundary lines in Fig. 1, one can obtain two critical values of  $k_z$ , namely,  $\pm k_z^w$ , as indicated in Fig. 1.  $\mathbf{k} = (0, 0, \pm k_z^w)$  are a pair of Weyl points, or 3D Dirac points, at which the conduction and valence bands touch. The appearance of Weyl points is usually attributed to accidental degeneracy or symmetry. [31–34] The obtained phase diagram in Fig. 1 sheds more light on its topological origin. At a given  $g$ , the Weyl points appear as two critical points separating a QH state of the effective 2D

system for  $|k_z| < k_z^w$  from an ordinary insulator state for  $|k_z| > k_z^w$ , at which the energy gap must vanish. Changing parameters cannot open energy gaps at the two Weyl points, unless they come together, so that the QH state in between is destroyed. At  $g = 0.2$ , the calculated energy spectra for four different  $k_z$  as functions of  $k_y$  are plotted in Fig. 5 for a semi-infinite sample with its surface parallel to the  $y$ - $z$  plane. It is found that for  $k_z < k_z^w$ , chiral surface states appear in the energy gap; the conduction and valence bands touch at  $k_z = k_z^w$ ; and for  $k_z > k_z^w$ , the energy gap reopens, but surface states no longer exist. These results are in good agreement with the phase diagram in Fig. 1. The chiral surface states appearing in the region of  $|k_z| < k_z^w$  give rise to the Fermi arcs. [31–34] The Weyl semimetals with Fermi arcs have been paid much attention recently. Our work suggests that a possible route to realize such an interesting 3D topological state of matter is through magnetic doping in 3D TIs.

This work is supported by the State Key Program for Basic Researches of China under Grants Nos. 2009CB929504 (LS), 2011CB922103, and 2010CB923400 (DYX), the National Natural Science Foundation of China under Grant Nos. 11225420, 11074110 (LS), 11074111 (RS), 11174125, 11074109, 91021003 (DYX), and a project funded by the PAPD of Jiangsu Higher Education Institutions. We also thank the US NSF Grants No. DMR-0906816 and No. DMR-1205734, and Princeton MRSEC Grant No. DMR-0819860 (DNS).

\* Electronic address: shengli@nju.edu.cn

† Electronic address: dyxing@nju.edu.cn

- [1] K. V. Klitzing, G. Dorda, and M. Pepper, Phys. Rev. Lett. **45**, 494 (1980).
- [2] D. C. Tsui, H. L. Stormer, and A. C. Gossard, Phys. Rev. Lett. **48**, 1559 (1982).
- [3] D. J. Thouless, M. Kohmoto, M. P. Nightingale, and M. den Nijs, Phys. Rev. Lett. **49**, 405 (1982); D. J. Thouless, J. Phys. C **17**, L325 (1984).
- [4] Q. Niu, D. J. Thouless, and Y. S. Wu, Phys. Rev. B. **31**, 3372 (1985).
- [5] F. D. M. Haldane, Phys. Rev. Lett. **61**, 2015 (1988).
- [6] C. L. Kane and E. J. Mele, Phys. Rev. Lett. **95**, 226801 (2005).
- [7] B. A. Bernevig, and S. C. Zhang, Phys. Rev. Lett. **96**, 106802 (2006).
- [8] B. A. Bernevig, T. L. Hughes, and S. C. Zhang, Science **314**, 1757 (2006).
- [9] M. König, S. Wiedmann, C. Brüne, A. Roth, H. Buhmann, L. W. Molenkamp, X. L. Qi, S. C. Zhang, Science **318**, 5851, 766 (2007).
- [10] L. Sheng, D. N. Sheng, C. S. Ting, and F. D. M. Haldane Phys. Rev. Lett. **95**, 136602 (2005).
- [11] C. Wu, B. A. Bernevig, and S. C. Zhang Phys. Rev. Lett. **96**, 106401 (2006).
- [12] C. L. Kane, and E. J. Mele, Phys. Rev. Lett. **95**, 146802 (2005).

- [13] D. N. Sheng, Z. Y. Weng, L. Sheng, and F. D. M. Haldane, Phys. Rev. Lett. **97**, 036808 (2006).
- [14] E. Prodan, Phys. Rev. B **80**, 125327 (2009); E. Prodan, New J. Phys. **12**, 065003 (2010).
- [15] H. C. Li, L. Sheng, D. N. Sheng, and D. Y. Xing, Phys. Rev. B **82**, 165104 (2010).
- [16] Y. Yang, Z. Xu, L. Sheng, B. G. Wang, D. Y. Xing, and D. N. Sheng Phys. Rev. Lett. **107**, 066602 (2011); H. C. Li, L. Sheng, and D.Y. Xing, Phys. Rev. Lett. **108**, 196806 (2012).
- [17] J. E. Moore, and L. Balents, Phys. Rev. B **75**, 121306 (R) (2007).
- [18] L. Fu and C. L. Kane, Phys. Rev. B **76**, 045302 (2007); L. Fu, C. L. Kane, E. J. Mele, Phys. Rev. Lett. **98**, 106803 (2007).
- [19] H. J. Zhang, C. X. Liu, X. L. Qi, X. Dai, Z. Fang, and S. C. Zhang, Nature Phys. **5**, 438(2009).
- [20] M. Z. Hasan and C. L. Kane, Rev. Mod. Phys. **82**, 3045 (2010).
- [21] X. L. Qi and S. C. Zhang, Physics Today. **63**, 33 (2010).
- [22] L. Fu and C. L. Kane, Phys. Rev. Lett. **100**, 096407 (2008).
- [23] X. L. Qi, T. Hughes, and S.-C. Zhang, Phys. Rev. B **78**, 195424 (2008).
- [24] A. M. Essin, J. E. Moore, and D. Vanderbilt, Phys. Rev.
- [25] D. Hsieh, *et al.*, Nature **452**, 970 (2008); D. Hsieh, *et al.*, Science **323**, 919 (2009).
- [26] Y. Xia, *et al.*, Nature Physics **5**, 398 (2009).
- [27] H. Zhang, C. Liu, X. Qi, X. Dai, Z. Fang, and S. Zhang, Nature Physics **5**, 438 (2009).
- [28] Y. L. Chen, *et al.*, Science **325**, 178 (2009).
- [29] P. Roushan, *et al.*, Nature **460**, 1106 (2009).
- [30] T. Zhang, *et al.*, Phys. Rev. Lett. **103**, 266803 (2009). Lett. **102**, 146805 (2009).
- [31] X. Wan, A. M. Turner, A. Vishwanath, and S. Y. Savrasov, Phys. Rev. B **83**, 205101 (2011).
- [32] A. Burkov and L. Balents, Phys. Rev. Lett., **107**, 127205 (2011).
- [33] K. Sun, W. V. Liu, A. Hemmerich and S. D. Sarma, Nature Physics **8**, 67 (2011).
- [34] C. Fang, M. J. Gilbert, X. Dai, and B. A. Bernevig, Phys. Rev. Lett. **108**, 266802 (2012).